Comput Mech (2015) 55:789–804
DOI 10.1007/s00466-015-1137-2

ORIGINAL PAPER

An analysis of a discontinuous spectral element method for elastic wave propagation in a heterogeneous material

Jonghoon Bin · William S. Oates · M. Yousuff Hussaini

Received: 19 April 2014 / Accepted: 16 February 2015 / Published online: 6 March 2015

Abstract The numerical dispersion and dissipation properties of a discontinuous spectral element method are investigated in the context of elastic waves in one dimensional periodic heterogeneous materials. Their frequency dependence and elastic band characteristics are studied. Dispersion relations representing both pass band and stop band structures are derived and used to assess the accuracy of the numerical results. A high-order discontinuous spectral Galerkin method is used to calculate the complex dispersion relations in heterogeneous materials. Floquet–Bloch theory is used to derive the elastic band structure. The accuracy of the dispersion relation is investigated with respect to the spectral polynomial orders for three different cases of materials. Numerical investigations illustrate a spectral convergence in numerical accuracy with respect to the polynomial order based on the elastic band structure and a discontinuous jump of the maximum resolvable frequency within the pass bands resulting in a step-like increase of it with respect to the polynomial order.

Keywords Dispersion relation · Floquet–Bloch theory · Band gap · Brillouin zone

J. Bin · W. S. Oates (✉)
Department of Mechanical Engineering,
Florida Center for Advanced Aero Propulsion (FCAAP),
Florida A&M/Florida State University,
Tallahassee, FL 32310-6046, USA
e-mail: woates@fsu.edu

J. Bin
e-mail: jbin@fsu.edu

M. Yousuff Hussaini
Department of Mathematics,
Florida State University, MCH413,
Tallahassee, FL 32306-4510, USA
e-mail: myh@math.fsu.edu

1 Introduction

Over the past decades, propagation of classical waves in composite heterogeneous materials with dielectric or elastic properties has been extensively studied to enhance understanding of the underlying physics with a view for a variety of applications including photonic and phononic devices [1–3]. These materials include granular materials, polycrystalline solids, alloys, ceramic composites, functionally graded materials, internally cracked materials, etc. When the wavelength of a wave propagating in the medium decreases and becomes comparable with the characteristic size of heterogeneities (e.g., microstructure length scale), the macroscopic waves experience dispersion and attenuation (i.e., phase and group velocities of the waves depend upon the wavelength) through locally successive reflections and transmissions of the waves at the interfaces of heterogeneities. A further decrease of the wavelength in a heterogeneous material reveals complex wave propagation characteristics: pass and stop frequency bands that are referred to as acoustic or phononic bands (by contrast with photonic bands for electromagnetic or optical waves in heterogeneous dielectric media) [4–6]. Thus, the heterogeneous material behaves like a discrete wave filter. For example, if the frequency of the wave lies within a stop band, the amplitude of the wave is macroscopically attenuated exponentially and so no propagation is possible through the material and hence the wave must be reflected totally.

The stop bands in heterogeneous elastic materials have been observed in experiments [7–11]. These phenomena have a great practical importance in science and engineering in mitigating vibration for high-precision mechanical systems, acoustic filters and noise control devices, ultrasonic transducers, etc. An accurate prediction of the phononic band gap in structures may also help design new composite materials

for a variety of structural dynamic and acoustic engineering applications.

When the structure is periodic, there exists a general method by which the dynamic behavior of the structure can be investigated. This method is based on Floquet theory of linear ordinary differential equations with periodic coefficients, and Bloch theory, originally propounded to describe the motion of a particle in a periodic potential (which may be considered to be a generalization of Floquet theory to three dimensions) [12]. This method has been applied to various problems with periodicity. For example, wave propagation in periodically laminated composite material with density variation in one dimension (1D) [13], in periodically triple-layered elastic medium in 1D [14], in a solid containing a periodic distribution of cracks in two dimensions [15], and in a periodic composite medium with a gas or liquid containing rigid spheres [16]. The solution of the eigenvalue problem is used to describe dispersion, modes and band gaps such as the stop band and the pass band.

Several methods for the calculation of the frequency band structure of phononic materials have been developed. The plane wave method (PWM) considers scalar problems for acoustic wave band structures as well as vector problems for elastic waves in plates containing periodic sets of inclusions [17]. This method has certain convergence problems especially in the case of fluid–solid composites and is also rather inefficient [18]. Korringa developed a multiple scattering method for the calculation of the energy of a Bloch wave with a reduced wave vector, which are obtained by the application of the dynamical theory of lattice interferences to electron waves [19]. Additional research was done by Kohn and Rostoker, who focused on the calculations of the electronic structure of solids [20]. The latter method appears to be numerically more efficient than PWM. However, the above methods are limited to infinite phononic materials made of non-dispersive lossless materials and cannot be directly applied to more realistic problems that often contain randomly distributed heterogeneous material characteristics, free surfaces, and complex geometry. As an alternative, finite-difference methods are often employed to determine the transmittance or reflectance of finite layers, which may be dispersive or dissipative. The well-known finite difference time domain (FDTD) method gives the transmission, reflection, and absorption coefficients of elastic waves incident on a finite slab of phononic crystals [21], but interpretation of the results, particularly for 3D systems with complex heterogeneities, is not straightforward because of the presence of spurious waves stemming from discretization. A discontinuous spectral element method (DSEM) is a desirable choice for handling wave propagation problems [22,23] as it is spectrally accurate and has relatively minimal dispersion and dissipation errors [24]. The spectral accuracy of DSEM distinguishes it from the traditional discontinuous Galerkin methods, with which it shares the attractive properties, such as easy accommodation of discontinuities at the interfaces and technically straightforward extension to 2D and 3D as well as microstructures of arbitrary material heterogeneities. For this particular application, we retain spectral accuracy when applying DSEM to heterogeneous material problems in comparison to other methods such as the finite element method (FEM) which have shown to exhibit different rates of convergence as a function of the order of the method and mesh size [25]. The DSEM scheme is well known to be efficient because the nodal points are the same as Gauss quadrature points and thus the interpolation and integration can be easily computed [22,23]. In addition, matrix manipulation in DSEM is much faster than FEM because DSEM updates all the variables in each local element and physical information is only transferred through the interfaces using the flux computation. Therefore DSEM provides a numerically efficient approach for the same level of accuracy using less grid points.

Numerical dispersion and dissipation errors due to the discretization of the governing equations complicate the interpretation of the numerical results, requiring a rigorous assessment of their accuracy. There are numerous studies of numerical accuracy including dispersion and dissipation errors for different numerical schemes [24,26–34] and these studies have been extended to 2D and 3D to determine the phononic and photonic band structures [29,30,35]. For elastic or electromagnetic wave propagation problems, most analyses of the dispersion relation have been primarily performed for periodic structures in the time domain [36,37] or the frequency domain [28–30,35]. To the authors' knowledge, no study has been conducted to understand the numerical dispersion and dissipation properties of models that simulate elastic band structures for elastic wave modes propagating in heterogeneous materials.

The present study focuses on the impact of discretization errors on the prediction of the physical dispersion relation and the band gap structures. Specifically, our objective is to study the numerical dispersion and dissipation errors in the semi-discrete version of the elastic wave equations for heterogeneous materials, which are spatially discretized using DSEM. We restrict our analysis to one dimension; however, the procedure can be directly extended to two or three dimensions. The one-dimensional analysis gives us a clear relation between the numerical accuracy and spatial order (or polynomial order (PN)) for a given periodic heterogeneous medium. Due to the existence of the band structure for the elastic wave propagating in the material with periodic heterogeneities (e.g., microstructures), the dispersion errors show different features relative to homogeneous materials. The Floquet–Bloch theory is used to obtain the band structure for the elastic wave propagating in the material with periodic microstructural heterogeneities.

The paper is organized as follows. The next section gives a mathematical model for one-dimensional elastic wave propagation including the numerical scheme chosen to discretize it. In Sect. 3, the dispersion relation of a one-dimensional periodic micro-structured heterogeneous material is derived using combined analytical and numerical methods. In Sect. 4, the numerical dispersion relation derived from the Floquet–Bloch theory is analyzed in three different cases. First, a homogeneous material is studied as a benchmark followed by two different types of periodic heterogeneous materials: (i) case 1 with the same propagation speed but different impedance and (i) case 2 with the same impedance but different propagation speed. In each case, the numerical result is compared with the analytic solution and the numerical accuracy is quantified in each case. Finally, the conclusions are given in Sect. 5.

2 Mathematical model for one-dimensional elastic wave propagation

2.1 Governing equations

Assuming sufficiently small deformation, the one-dimensional elastic wave equations can be written in conservative form as a first-order variable coefficient linear hyperbolic system

$$\frac{\partial \mathbf{u}}{\partial t} + \frac{\partial \mathbf{f}(\mathbf{u})}{\partial x} = 0, \tag{1}$$

$$\mathbf{u} = \begin{bmatrix} u_1 \\ u_2 \end{bmatrix} = \begin{bmatrix} \varepsilon \\ \rho v \end{bmatrix},$$

$$\mathbf{f}(\mathbf{u}) = \mathbf{A}\mathbf{u} = \begin{bmatrix} 0 & -1/\rho \\ -K & 0 \end{bmatrix} \begin{bmatrix} u_1 \\ u_2 \end{bmatrix}, \tag{2}$$

where $\varepsilon(x,t)$ is the strain, $v(x,t)$ is the velocity, and x and t are the spatial and temporal coordinates, respectively. Both the density of the solid, $\rho(x)$, and the Young's modulus, $K(x)$, vary spatially.

2.2 Numerical method

In the DSEM [22], the physical spatial domain Ω is divided into M elements, $\Omega = \cup_{n=1}^{\mathrm{M}} \Omega_n$. In each element, a spectral representation based on p-th order interpolants is used. So, the solution in $\Omega_n = [x_{n-1}, x_n]$, $\mathbf{u}^n(x)$, is approximated by

$$\mathbf{u}^n(x,t) \approx \mathbf{u}_h^n(x,t) = \sum_{k=0}^{\mathrm{p}} \mathbf{C}_k^n(t) l_k^n(x) \quad \text{in} \quad \Omega_n\,, \tag{3}$$

where $\mathbf{C}_k^n$ are the nodal values in the element Ω_n and $l_k^n(x)$ is basis Lagrange polynomials for the element Ω_n

$$l_k^n(x) = \prod_{\substack{l=0 \\ l \neq k}}^{\mathrm{p}} \frac{(x - x_l)}{(x_k - x_l)}, \tag{4}$$

where the nodal points x_l in $\Omega_n^{(i)}$ are chosen to be the nodes of the Legendre–Gauss quadrature and p is the highest order of polynomials for the chosen basis.

Multiplying Eq. (1) by $l_k^n(x)$ and integrating over the element Ω_n yields the weak formulation [22]

$$\int_{x_{n-1}}^{x_n} \left[\frac{\partial \mathbf{u}_h^n}{\partial t} + \frac{\partial}{\partial x}(\mathbf{A}^n \mathbf{u}_h^n) \right] l_k^n(x)\, \mathrm{d}x = 0$$
$$\text{for } k = 0, 1, 2, \ldots, \mathrm{p} \text{ in } \Omega_n. \tag{5}$$

Using integration by parts, Eq. (5) becomes

$$\int_{x_{n-1}}^{x_n} \frac{\partial \mathbf{u}_h^n}{\partial t} l_k^n(x)\, \mathrm{d}x + \left[\mathbf{f}^{\mathrm{RL}} l_k^n(x) \right]_{x_{n-1}}^{x_n}$$
$$- \int_{x_{n-1}}^{x_n} (\mathbf{A}^n \mathbf{u}_h^n) \frac{\partial l_k^n(x)}{\partial t} \mathrm{d}x = 0, \tag{6}$$

where $\mathbf{f}^{\mathrm{RL}}(\mathbf{u}_{\mathrm{L}}, \mathbf{u}_{\mathrm{R}})$ is the flux at the interface, and $\mathbf{u}_{\mathrm{L}}$ and $\mathbf{u}_{\mathrm{R}}$ are respectively the left and the right values of $\mathbf{u}$ at the interfaces of the element Ω_n interpolated from the values at interior nodal points. Several kinds of flux formulae have been suggested to compute the flux at the interface [22–24, 26]. Commonly used ones are the characteristics-based flux formula for a linear system

$$\mathbf{f}^{\mathrm{RL}}(\mathbf{u}_{\mathrm{L}}, \mathbf{u}_{\mathrm{R}}) = \frac{1}{2} \left[\mathbf{f}(\mathbf{u}_{\mathrm{L}}) + \mathbf{f}(\mathbf{u}_{\mathrm{R}}) - \theta |\mathbf{A}| (\mathbf{u}_{\mathrm{R}} - \mathbf{u}_{\mathrm{L}}) \right], \quad \theta \geq 0, \tag{7}$$

where $\mathbf{f}(\mathbf{u}) = \mathbf{A}\mathbf{u}$. Equation (7) is called the Roe flux when $\theta = 1$ and a centered flux when $\theta = 0$ [24,38]. For convenience, Eq. (7) can be reformulated as

$$\mathbf{f}^{\mathrm{RL}}(\mathbf{u}_{\mathrm{L}}, \mathbf{u}_{\mathrm{R}}) = \mathbf{A}_{\mathrm{L}} \mathbf{u}_{\mathrm{L}} + \mathbf{A}_{\mathrm{R}} \mathbf{u}_{\mathrm{R}}, \quad \theta \geq 0, \tag{8}$$

where $\mathbf{A}_{\mathrm{L}} = \frac{1}{2}[\mathbf{A} + \theta|\mathbf{A}|]$ and $\mathbf{A}_{\mathrm{R}} = \frac{1}{2}[\mathbf{A} - \theta|\mathbf{A}|]$. Equation (1) being linear, the flux terms can be further simplified as [38,39]

$$\mathbf{A}_{\mathrm{L}} = \begin{bmatrix} c^{(\mathrm{L})} Z_{\mathrm{L}} & -\frac{c^{(\mathrm{L})}}{Z_{\mathrm{L}} + Z_{\mathrm{R}}} \\ -\frac{c^{(\mathrm{L})}}{Y_{\mathrm{L}} + Y_{\mathrm{R}}} & \frac{c^{(\mathrm{L})}}{(Y_{\mathrm{L}} + Y_{\mathrm{R}}) Z_{\mathrm{L}}} \end{bmatrix}, \quad \mathbf{A}_R = \begin{bmatrix} -c^{(\mathrm{R})} Z_{\mathrm{R}} & -\frac{c^{(\mathrm{R})}}{Z_{\mathrm{L}} + Z_{\mathrm{R}}} \\ -\frac{c^{(\mathrm{R})}}{Y_{\mathrm{L}} + Y_{\mathrm{R}}} & \frac{c^{(\mathrm{R})}}{(Y_{\mathrm{L}} + Y_{\mathrm{R}}) Z_{\mathrm{R}}} \end{bmatrix}, \tag{9}$$

where $Y = 1/Z$, $Z = \rho c = \sqrt{\rho K}$, c is longitudinal wave speed, and the sub- and the super-scripts denoted by L and R represent the left and the right values of the interface, respec-

tively. So, the semi-discrete form of Eq. (6) can be written as

$$\int_{x_{n-1}}^{x_n} \frac{\partial \mathbf{u}_h^n}{\partial t} l_k^n(x)\mathrm{d}x + \left[\mathbf{A}_{\mathrm{L}}^n \mathbf{u}_h^n(x_n,t) + \mathbf{A}_{\mathrm{R}}^{n+1}\mathbf{u}_h^{n+1}(x_n,t)\right] l_k^n(x_n) - \left[\mathbf{A}_{\mathrm{L}}^{n-1}\mathbf{u}_h^{n-1}(x_{n-1},t) + \mathbf{A}_{\mathrm{R}}^n \mathbf{u}_h^n(x_{n-1},t)\right] l_k^n(x_{n-1}) - \int_{x_{n-1}}^{x_n} (\mathbf{A}^n \mathbf{u}_h^n) \frac{\partial l_k^n(x)}{\partial x}\mathrm{d}x = 0, \tag{10}$$

for $k = 0, 1, 2, \ldots, \mathrm{p}$ in Ω_n.

Now, we map the physical domain onto the computational domain

$$\xi(x) : \Omega_n = [x_{n-1}, x_n] \to \Omega_{\mathrm{c}}[-1, 1], \quad \xi = \frac{2}{\delta}(x - x_{\mathrm{c}}), \tag{11}$$

where $\delta = (x_n - x_{n-1})$ and $x_{\mathrm{c}} = (x_{n-1} + x_n)/2$. The basis functions are the same for all the elements when expressed in the local coordinate ξ, $l_k^n(x) = L_k(\xi)$. If the mapping of Eq. (11) is introduced into Eq. (10), one obtains

$$\sum_{l=0}^{\mathrm{p}} \left\{ \frac{\delta}{2}\frac{\partial \mathbf{C}_l^n}{\partial t}\int_{-1}^{1} L_l(\xi)L_k(\xi)\mathrm{d}\xi + \left[\mathbf{A}_{\mathrm{L}}^n \mathbf{C}_l^n L_l(1)L_k(1) + \mathbf{A}_{\mathrm{R}}^{n+1}\mathbf{C}_l^{n+1}L_l(-1)L_k(1)\right] - \left[\mathbf{A}_{\mathrm{L}}^{n-1}\mathbf{C}_l^{n-1}L_l(1)L_k(-1) + \mathbf{A}_{\mathrm{R}}^n \mathbf{C}_l^n L_l(-1)L_k(-1)\right] - \mathbf{A}^n\mathbf{C}_l^n \int_{-1}^{1} L_l(\xi)\frac{\partial L_k(\xi)}{\partial \xi}\mathrm{d}\xi \right\} = 0, \tag{12}$$

for $k = 0, 1, \ldots, \mathrm{p}$ in Ω_n. For time advancement in Eq. (12), explicit third-order Runge–Kutta scheme is used [22].

One significant advantage of DSEM is that it allows physical variables to be discontinuous at interfaces, which is crucial in the simulation of the elastic wave propagation in randomly distributed heterogeneous materials. One can simply use each partitioned element to model each microstructure in the medium with different physical parameters.

In the next section, we analytically derive the physical dispersion relation of one-dimensional periodic heterogeneous materials and numerically determine it using the DSEM scheme applied to heterogeneous materials, which may lead to errors due to numerical dispersion and dissipation errors of the numerical scheme chosen in the study and this relation is verified by the benchmark solutions for the homogeneous and the heterogeneous cases (Fig. 1).

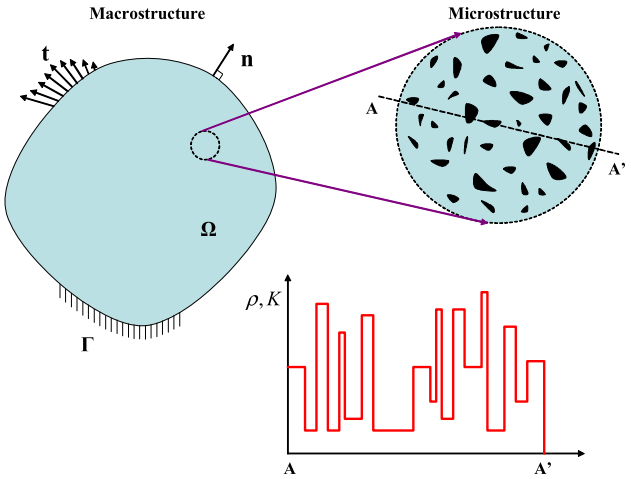

Fig. 1 One-dimensional modeling of heterogeneous materials

3 Dispersion relation of a one-dimensional periodic micro-structured heterogeneous materials

3.1 Theoretical model

Let us consider longitudinal waves propagating in the x-direction through a spatially infinite periodic heterogeneous rod consisting of layers of two elastic materials $\Omega_0^{(1)}$ and $\Omega_1^{(2)}$ (see Fig. 2). Then, the governing equation in the absence of body forces is

$$\frac{\partial}{\partial x}\left[K(x)\frac{\partial u(x,t)}{\partial x}\right] - \rho(x)\frac{\partial^2 u(x,t)}{\partial t^2} = 0, \tag{13}$$

where $u(x,t)$ is the displacement of the rod at the longitudinal coordinate x and at time t. The material properties can be described by the following periodic function of period $l = l_1 + l_2$ (see Fig. 2):

$$\rho(x) = \begin{cases} \rho_1, \\ \rho_2, \end{cases} \quad K(x) = \begin{cases} K_1, & -l_1 < x < 0 \text{ in } \Omega_0^{(1)} \\ K_2, & 0 < x < l_2 \text{ in } \Omega_0^{(2)} \end{cases}. \tag{14}$$

For time harmonic vibration of frequency ω, the solution has the form $u(x,t) = U(x)\mathrm{e}^{\mathrm{j}\omega t}$. Then, substituting this expres-

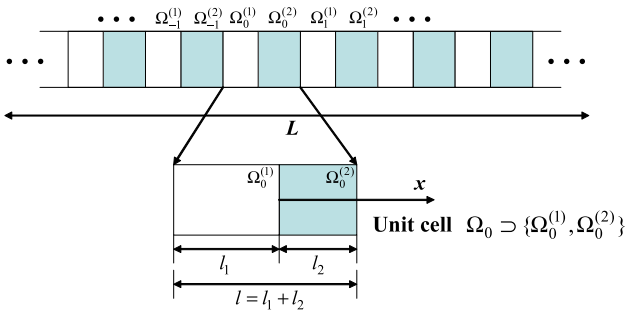

Fig. 2 Geometry of a periodic heterogeneous composite material with piecewise constant properties

sion to Eq. (13) yields

$$K^{(s)}\frac{\mathrm{d}^2U_n^{(s)}}{\mathrm{d}x^2}+\rho^{(s)}\omega^2U_n^{(s)}=0 \text{ in } \Omega_n^{(s)},\quad s=1,2,\quad n\in Z, \tag{15}$$

where $U_n^{(s)}$ is the displacement amplitude in each layer in the domain $\Omega_n^{(s)}$. Equation (15) has to satisfy the continuity of the displacement and the stress at the interfaces:

$$U_n^{(1)}=U_n^{(2)},\ K^{(1)}\frac{\mathrm{d}U_n^{(1)}}{\mathrm{d}x}=K^{(2)}\frac{\mathrm{d}U_n^{(2)}}{\mathrm{d}x},\quad n\in Z. \tag{16}$$

We assume that the displacement satisfies the quasi-periodicity condition for time harmonic wave propagating through a periodic composite material. According to the Floquet–Bloch approach [12], the solution can be represented in the form

$$u_n^{(s)}(x,t)=F_n^{(s)}(x)\mathrm{e}^{\mathrm{j}\mu x}\mathrm{e}^{\mathrm{j}\omega t}, \tag{17}$$

where ω is the frequency, μ is the Bloch wavenumber in the superscript, $\mathrm{j}=\sqrt{-1}$, and $F_n^{(s)}(x)$ is a spatially periodic function used to describe the influence of the composite microstructure, $F_n^{(s)}(x)=F_{n+1}^{(s)}(x+l)$. The periodicity of $F_n^{(s)}(x)$ leads to

$$U_{n+1}^{(s)}(x+l)=U_n^{(s)}(x)\mathrm{e}^{\mathrm{j}\mu l} \text{ in } \Omega_n^{(s)},\ (s-2)l_1+nl<x<(s-1)l_2+nl,\ s=1,2,\ n\in Z. \tag{18}$$

The physical meaning of the propagation wavenumber μ can be found from the application of the Floquet theory shown in Brillouin [5,6]. The nature of wave propagation inside the material depends upon the value of the Bloch wavenumber μ, which relates the displacement of any two points separated by a distance l inside the material s. Assuming $\mu=\mu_\mathrm{R}+\mathrm{j}\mu_\mathrm{I}$, Eq. (17) is rewritten

$$u_n^{(s)}(x,t)=F_n^{(s)}(x)\mathrm{e}^{\mathrm{j}\mu_\mathrm{R}x}\mathrm{e}^{-\mu_\mathrm{I}x}\mathrm{e}^{\mathrm{j}\omega t}. \tag{19}$$

It is apparent from Eq. (19) that the wave attenuates exponentially if $\mu_I>0$. Such frequency bands are called stop bands since all the waves attenuate as they propagate through the periodic material, while the bands where $\mu_\mathrm{I}=0$ are called pass bands. This result describes the existence of phononic band gaps.

The general solution can also be represented by

$$u_n^{(s)}(x,t)=U_n^{(s)}(x)\mathrm{e}^{\mathrm{j}\omega t}=\left[A_n^{(s)}(x)\mathrm{e}^{\mathrm{j}\alpha^{(s)}\omega x}+B_n^{(s)}(x)\mathrm{e}^{-\mathrm{j}\alpha^{(s)}\omega x}\right]\mathrm{e}^{\mathrm{j}\omega t}, \tag{20}$$

where $\alpha^{(s)}=\sqrt{\rho^{(s)}/K^{(s)}}$, $s=1,2$, $n\in Z$, $(s-2)l_1+nl<x<(s-1)l_2+nl$. Equation (18) that expresses the periodicity of the layered materials between the domains $\Omega_0^{(2)}$ and $\Omega_1^{(1)}$ and Eq. (16) that imposes the continuity of the displacement and stress at the interfaces between the domains $\Omega_0^{(1)}$ and $\Omega_0^{(2)}$, together determine all the coefficients $\{A_0^{(1)},A_0^{(2)},B_0^{(1)},B_0^{(2)}\}$. This results in the homogeneous system

$$\mathbf{M}_\mathrm{th}\left\{A_0^{(1)},A_0^{(2)},B_0^{(1)},B_0^{(2)}\right\}^\mathrm{T}=0, \tag{21}$$

where

$$\mathbf{M}_\mathrm{th}=\begin{bmatrix}1 & -1 & 1 & -1\\ k^{(1)}K^{(1)} & -k^{(2)}K^{(2)} & -k^{(1)}K^{(1)} & k^{(2)}K^{(2)}\\ \mathrm{e}^{\mathrm{j}(\mu l-k^{(1)}l_1)} & -\mathrm{e}^{\mathrm{j}k^{(2)}l_2} & \mathrm{e}^{\mathrm{j}(\mu l+k^{(1)}l_1)} & -\mathrm{e}^{-\mathrm{j}k^{(2)}l_2}\\ k^{(1)}K^{(1)}\mathrm{e}^{\mathrm{j}(\mu l-k^{(1)}l_1)} & -k^{(2)}K^{(2)}\mathrm{e}^{\mathrm{j}k^{(2)}l_2} & -k^{(1)}K^{(1)}\mathrm{e}^{\mathrm{j}(\mu l+k^{(1)}l_1)} & k^{(2)}K^{(2)}\mathrm{e}^{-\mathrm{j}k^{(2)}l_2}\end{bmatrix} \tag{22}$$

and $k^{(s)}=\alpha^{(s)}\omega$, $s=1,2$.

System of Eq. (21) has a non-trivial solution if and only if the determinant of the matrix $\mathbf{M}_\mathrm{th}$ is zero, which yields the dispersion equation relating μ and ω, and it may be written in the form

$$\cos(\mu l)=\cos(\omega\alpha^{(1)}l_1)\cos(\omega\alpha^{(2)}l_2)-\frac{1}{2}\left(\frac{Z_1}{Z_2}+\frac{Z_2}{Z_1}\right)\sin(\omega\alpha^{(1)}l_1)\sin(\omega\alpha^{(2)}l_2), \tag{23}$$

where $Z_s=\rho^{(s)}c^{(s)}=\rho^{(s)}/\alpha^{(s)}=\sqrt{\rho^{(s)}K^{(s)}}$, $s=1,2$. For a homogeneous material, we have $l=l_1+l_2$, $\alpha=\alpha_1=\alpha_2$, and $Z_1=Z_2$. Equation (23) then yields the linear dispersion relation, $\mu=\alpha\omega$.

Figure 3 graphically represents the dispersion relation of an elastic wave in a one-dimensional periodic heterogeneous material. Physical values used in this case are $(\rho^{(1)},K^{(1)})=(1,1)$, $(\rho^{(2)},K^{(2)})=(1,3)$, and $l_1=0.5l$. Then, $c^{(1)}=1$, $c^{(2)}=\sqrt{3}$, $Z_1=1$, and $Z_2=\sqrt{3}$. Impedance mismatch due to the existence of heterogeneities (microstructures) in the medium gives rise to locally successive reflections and transmissions of the elastic waves at the interface, which finally results in band gap phenomena as shown in Fig. 3. According to Bloch's theory, the effective

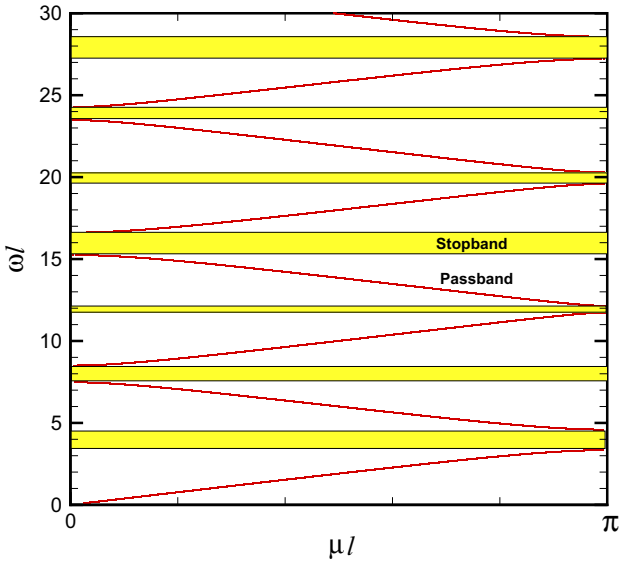

Fig. 3 Dispersion curves of a 1D periodic heterogeneous medium

wavenumber, μ, ranges from 0 to π lying on the first Brillouin zone. As seen in this figure, unlike the linear wave propagation in homogeneous medium, (i.e., $\mu = \alpha\omega$ from Eq. (23)), the phase velocity (ω/μ) and the group velocity $(\mathrm{d}\omega/\mathrm{d}\mu)$ are not constant along the propagation direction due to the periodic variations in material properties. The regions identified with the yellow strips represent stop bands, and waves with corresponding frequencies do not propagate through the structure.

Alternative to the analytic approach, numerical simulation can determine the band gap or dispersion relation in heterogeneous materials. It is proper to emphasize that in most practical cases, numerical solution is the only choice due to the complexity of the microstructural media. In such cases, a rigorous assessment of the numerical accuracy is needed.

3.2 Numerical model

We consider periodic one-dimensional linear elastic wave propagation in a medium. Equation (1) can be written in the frequency domain (using $\mathbf{u}(x,t) = \hat{\mathbf{u}}(x)\mathrm{e}^{\mathrm{j}\omega t}$)

$$\mathrm{j}\omega\hat{\mathbf{u}} + \frac{\partial \mathbf{f}(\hat{\mathbf{u}})}{\partial x} = \mathrm{j}\omega\hat{\mathbf{u}} + \frac{\partial}{\partial x}(\mathbf{A}\hat{\mathbf{u}}) = 0, \tag{24}$$

where $\hat{\mathbf{u}}$ is an $\mathrm{N}\times 1$ vector where N is the number of dependent variables, $\mathbf{A}$ is an $\mathrm{N}\times\mathrm{N}$ matrix in general In the DSEM, the physical spatial domain (Ω) is divided into M elements, $\Omega = \cup_{n=1}^{\mathrm{M}}\Omega_n$ where Ω_n is a unit cell, $\Omega_n \supset [\Omega_n^{(1)}, \Omega_n^{(2)}]$, and n is the element index, satisfying the periodicity of a heterogeneous composite material (see Fig. 2). We seek a Floquet–Bloch solution to Eq. (24) in the form

$$\hat{\mathbf{u}}(x) = \mathbf{F}(x)\mathrm{e}^{\mathrm{j}\mu x}, \tag{25}$$

where $\mathbf{F}(x)$ is a periodic function on Ω_n and μ is an effective wavenumber satisfying periodicity on Ω_n. Substituting Eq. (25) into Eq. (24), we get

$$\mathrm{j}\omega\mathbf{F} + \left(\frac{\partial}{\partial x} + \mathrm{j}\mu\right)(\mathbf{AF}) = 0 \ \text{ in } \ \Omega_n. \tag{26}$$

The spatial domain is partitioned into non-overlapping elements, $\Omega_n^{(i)}$ where $n = 1, 2, \ldots, \mathrm{M}$ and $i = 1, 2$. For simplicity, we just consider the unit cell $\Omega_n \supset [\Omega_n^{(1)}, \Omega_n^{(2)}]$ satisfying the periodicity of $\mathbf{F}(x)$ where $\Omega_n^{(1)} = [x_{n-1}, x_n] = [nl - l_1, nl]$ and $\Omega_n^{(2)} = [x_n, x_{n+1}] = [nl, nl + l_2]$ (see Fig. 2).

In each element, a spectral representation based on p-th order interpolants is used. Thus, the periodic function on Ω_n, $\mathbf{F}^{n,i}(x)$, is approximated by

$$\mathbf{F}^{n,i}(x) \approx \mathbf{F}_h^{n,i}(x) = \sum_{k=0}^{\mathrm{p}} \mathbf{C}_k^{n,i} l_k^{n,i}(x) \ \text{ in } \ \Omega_n^{(i)}, \quad i = 1, 2, \tag{27}$$

where $l_k^{n,i}(x)$ is basis Lagrange polynomials for element $\Omega_n^{(i)}$ given in Eq. (4), p is the highest order of polynomials in the chosen basis, and $\mathbf{C}_k^{n,i}$ are the nodal values at x_k, which are the nodal points in $\Omega_n^{(i)}$.

Multiplying Eq. (26) by $l_k^{n,i}(x)$ and integrating over $\Omega_n^{(i)}$, we obtain the weak form

$$\int_{x_{n+i-2}}^{x_{n+i-1}} \left(\mathrm{j}\omega\mathbf{F}_h^{n,i} + \mathrm{j}\mu(\mathbf{A}^{n,i}\mathbf{F}_h^{n,i}) + \frac{\partial}{\partial x}(\mathbf{A}^{n,i}\mathbf{F}_h^{n,i})\right) l_k^{n,i}(x)\mathrm{d}x = 0 \quad \text{in } \Omega_n^{(i)}, \quad i = 1, 2, \tag{28}$$

for $k = 0, 1, 2, \ldots, \mathrm{p}$. By applying integration by parts to Eq. (28), we get

$$\int_{x_{n+i-2}}^{x_{n+i-1}} \left(\mathrm{j}\omega\mathbf{F}_h^{n,i} + \mathrm{j}\mu(\mathbf{A}^{n,i}\mathbf{F}_h^{n,i})\right) l_k^{n,i}(x)\mathrm{d}x + \left[\mathbf{f}^{\mathrm{RL}} l_k^{n,i}(x)\right]_{x_{n+i-2}}^{x_{n+i-1}} - \int_{x_{n+i-2}}^{x_{n+i-1}} (\mathbf{A}^{n,i}\mathbf{F}_h^{n,i}) \frac{\partial l_k^{n,i}(x)}{\partial x}\mathrm{d}x = 0, \tag{29}$$

where $\mathbf{f}^{\mathrm{RL}}(\mathbf{F}_{\mathrm{L}}, \mathbf{F}_{\mathrm{R}})$ is the flux vector at the interface given by Eq. (8). The semi-discrete form of Eq. (29) can be written as

$$\int_{x_{n-1}}^{x_n} \left(\mathrm{j}\omega\mathbf{F}_h^{n,1} + \mathrm{j}\mu(\mathbf{A}^{n,1}\mathbf{F}_h^{n,1})\right) l_k^{n,1}(x)\mathrm{d}x + \left[\mathbf{A}_{\mathrm{L}}^{n,1}\mathbf{F}_h^{n,1}(x_n, t) + \mathbf{A}_{\mathrm{R}}^{n,2}\mathbf{F}_h^{n,2}(x_n, t)\right] l_k^{n,1}(x_n) - \left[\mathbf{A}_{\mathrm{L}}^{n-1,2}\mathbf{F}_h^{n-1,2}(x_{n-1}, t) + \mathbf{A}_{\mathrm{R}}^{n,1}\mathbf{F}_h^{n,1}(x_{n-1}, t)\right] l_k^{n,1}(x_{n-1})$$

$$-\int_{x_{n-1}}^{x_n}(\mathbf{A}^{n,1}\mathbf{F}_h^{n,1})\frac{\partial l_k^{n,1}(x)}{\partial x}\mathrm{d}x=0 \quad \text{in } \Omega_n^{(1)}, \tag{30}$$

$$\int_{x_n}^{x_{n+1}}\left(\mathrm{j}\omega\mathbf{F}_h^{n,2}+\mathrm{j}\mu(\mathbf{A}^{n,2}\mathbf{F}_h^{n,2})\right)l_k^{n,2}(x)\mathrm{d}x + \left[\mathbf{A}_{\mathrm{L}}^{n,2}\mathbf{F}_h^{n,2}(x_{n+1},t)+\mathbf{A}_{\mathrm{R}}^{n+1,1}\mathbf{F}_h^{n+1,1}(x_{n+1},t)\right]l_k^{n,2}(x_{n+1}) - \left[\mathbf{A}_{\mathrm{L}}^{n,1}\mathbf{F}_h^{n,1}(x_n,t)+\mathbf{A}_{\mathrm{R}}^{n,2}\mathbf{F}_h^{n,2}(x_n,t)\right]l_k^{n,2}(x_n) - \int_{x_n}^{x_{n+1}}(\mathbf{A}^{n,2}\mathbf{F}_h^{n,2})\frac{\partial l_k^{n,2}(x)}{\partial x}\mathrm{d}x=0 \quad \text{in } \Omega_n^{(2)}, \tag{31}$$

for $k=0,1,2,\ldots,\mathrm{p}$.

We now map the physical domain onto the computational domain

$$\xi(x):\Omega_n^{(i)}=[x_{n+i-2},\ x_{n+i-1}]\rightarrow\Omega_c[-1,\ 1],\qquad \xi=\frac{2}{\delta_i}(x-x_c), \tag{32}$$

where $\delta_i=(x_{n+i-1}-x_{n+i-2})$, $x_c=(x_{n+i-1}+x_{n+i-2})/2$ and $l_k^{n,i}(x)=L_k(\xi)$.

Substitution of Eq. (27) into Eqs. (30) and (31) leads to

$$\sum_{l=0}^{\mathrm{p}}\left\{\frac{\mathrm{j}\delta_1}{2}(\omega\mathbf{I}+\mu\mathbf{A}^{n,1})\mathbf{C}_l^{n,1}\int_{-1}^{1}L_l(\xi)L_k(\xi)\mathrm{d}\xi + \left[\mathbf{A}_{\mathrm{L}}^{n,1}\mathbf{C}_l^{n,1}L_l(1)L_k(1)+\mathbf{A}_{\mathrm{R}}^{n,2}\mathbf{C}_l^{n,2}L_l(-1)L_k(1)\right] - \left[\mathbf{A}_{\mathrm{L}}^{n-1,2}\mathbf{C}_l^{n-1,2}L_l(1)L_k(-1)+\mathbf{A}_{\mathrm{R}}^{n,1}\mathbf{C}_l^{n,1}L_l(-1)L_k(-1)\right] -\mathbf{A}^{n,1}\mathbf{C}_l^{n,1}\int_{-1}^{1}L_l(\xi)\frac{\partial L_k(\xi)}{\partial\xi}\mathrm{d}\xi\right\}=0 \quad \text{in } \Omega_n^{(1)}, \tag{33}$$

$$\sum_{l=0}^{\mathrm{p}}\left\{\frac{\mathrm{j}\delta_2}{2}(\omega\mathbf{I}+\mu\mathbf{A}^{n,2})\mathbf{C}_l^{n,2}\int_{-1}^{1}L_l(\xi)L_k(\xi)\mathrm{d}\xi + \left[\mathbf{A}_{\mathrm{L}}^{n,2}\mathbf{C}_l^{n,2}L_l(1)L_k(1)+\mathbf{A}_{\mathrm{R}}^{n+1,1}\mathbf{C}_l^{n+1,1}L_l(-1)L_k(1)\right] - \left[\mathbf{A}_{\mathrm{L}}^{n,1}\mathbf{C}_l^{n,1}L_l(1)L_k(-1)+\mathbf{A}_{\mathrm{R}}^{n,2}\mathbf{C}_l^{n,2}L_l(-1)L_k(-1)\right] -\mathbf{A}^{n,2}\mathbf{C}_l^{n,2}\int_{-1}^{1}L_l(\xi)\frac{\partial L_k(\xi)}{\partial\xi}\mathrm{d}\xi\right\}=0 \quad \text{in } \Omega_n^{(2)}, \tag{34}$$

for $k=0,1,\ldots,\mathrm{p}$. Due to the periodicity on Ω_n, i.e., $\mathbf{A}_{\mathrm{L}}^{n-1,2}\mathbf{C}_l^{n-1,2}=\mathbf{A}_{\mathrm{L}}^{n,2}\mathbf{C}_l^{n,2}$ and $\mathbf{A}_{\mathrm{R}}^{n+1,1}\mathbf{C}_l^{n+1,1}=\mathbf{A}_{\mathrm{R}}^{n,1}\mathbf{C}_l^{n,1}$, Eqs. (33) and (34) can be expressed in the matrix form

$$\begin{bmatrix}\mathbf{N}_{11}&\mathbf{N}_{12}\\ \mathbf{N}_{21}&\mathbf{N}_{22}\end{bmatrix}\begin{Bmatrix}\mathbf{C}^{n,1}\\ \mathbf{C}^{n,2}\end{Bmatrix}=\begin{bmatrix}-\mathbf{B}_1\mathbf{Q}_1&0\\ 0&-\mathbf{B}_2\mathbf{Q}_2\end{bmatrix}\begin{Bmatrix}\mathbf{C}^{n,1}\\ \mathbf{C}^{n,2}\end{Bmatrix} \tag{35}$$

where

$$\mathbf{C}^{n,k}=[\mathbf{C}_0^{n,k},\mathbf{C}_1^{n,k},\ldots,\mathbf{C}_{\mathrm{p}}^{n,k}]^{\mathrm{T}},\ k=1,2,$$

$$\{B_k\}_{lm}=\frac{\mathrm{j}\delta_k}{2}(\omega\mathbf{I}+\mu\mathbf{A}^{n,k}),$$

$$\{Q_k\}_{lm}=\mathbf{I}\int_{-1}^{1}L_l(\xi)L_m(\xi)\mathrm{d}\xi,$$

$$\{N_{11}\}_{lm}=\mathbf{A}_{\mathrm{L}}^{n,1}L_l(1)L_m(1)-\mathbf{A}_{\mathrm{R}}^{n,1}L_l(-1)L_m(-1) -\mathbf{A}^{n,1}\int_{-1}^{1}L_m(\xi)\frac{\partial L_l(\xi)}{\partial\xi}\mathrm{d}\xi,$$

$$\{N_{12}\}_{lm}=-\mathbf{A}_{\mathrm{L}}^{n,2}L_m(1)L_l(-1)+\mathbf{A}_{\mathrm{R}}^{n,2}L_m(-1)L_l(1),$$

$$\{N_{21}\}_{lm}=-\mathbf{A}_{\mathrm{L}}^{n,1}L_m(1)L_l(-1)+\mathbf{A}_{\mathrm{R}}^{n,1}L_m(-1)L_l(1),$$

$$\{N_{22}\}_{lm}=\mathbf{A}_{\mathrm{L}}^{n,2}L_l(1)L_m(1)-\mathbf{A}_{\mathrm{R}}^{n,2}L_l(-1)L_m(-1) -\mathbf{A}^{n,2}\int_{-1}^{1}L_m(\xi)\frac{\partial L_l(\xi)}{\partial\xi}\mathrm{d}\xi,$$

where $l,m=0,1,\ldots,\mathrm{p}$. (36)

This is a fundamental eigenvalue problem of the form $\mathbf{AX}=\mathbf{\Lambda X}$ where $\mathbf{\Lambda}$ is a diagonal eigenvalue matrix since $\mathbf{Q}_1$ and $\mathbf{Q}_2$ are diagonal from Eq. (36). Equation (35) has a non-trivial solution if its determinant is zero, which leads to the numerical dispersion relation

$$\det\mathbf{M}_{\mathrm{num}}=0 \text{ where } \mathbf{M}_{\mathrm{num}}=\begin{pmatrix}\mathbf{B}_1\mathbf{Q}_1+\mathbf{N}_{11}&\mathbf{N}_{12}\\ \mathbf{N}_{21}&\mathbf{B}_2\mathbf{Q}_2+\mathbf{N}_{22}\end{pmatrix}. \tag{37}$$

In one-dimensional problems, $\mathbf{M}_{\mathrm{num}}$ is $[2\mathrm{N}\times(\mathrm{p}+1)]$ by $[2\mathrm{N}\times(\mathrm{p}+1)]$ matrix where $\mathrm{N}=2$ and Eq. (37) results in $[2\mathrm{N}\times(\mathrm{p}+1)]$-th order polynomials for the Bloch wavenumber μ. For a given frequency, it is possible to determine the Bloch wavenumber μ by solving Eq. (37).

4 Analysis of numerical dispersion

4.1 Wave propagation in a homogeneous material: $Z_1=Z_2$ and $c^{(1)}=c^{(2)}$

As a stringent test case for the numerical method, we choose the homogeneous material parameter set: $\rho^{(1)}=1$, $K^{(1)}=1$, $\rho^{(2)}=1$, and $K^{(2)}=1$ which gives $Z_1=Z_2=1$ and $c^{(1)}=c^{(2)}=1$. The exact solution for this case has the phase and the group velocities constant in the whole range of wavenumbers. The dissipation and dispersion errors of the DSEM affect the numerical values of phase and group velocities. The numerical dispersion relation of DSEM is given in Appendix to distinguish its effect relative to physical dis-

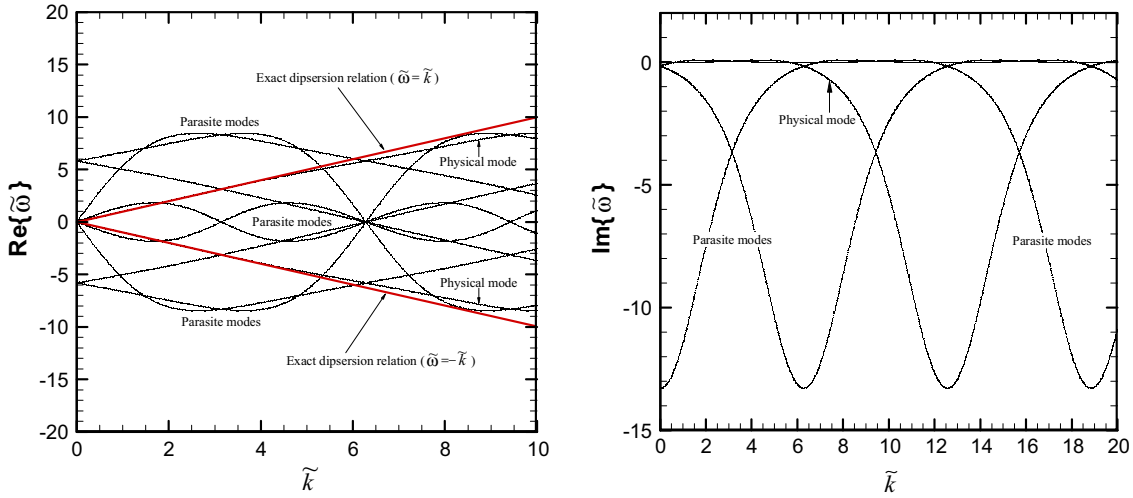

Fig. 4 Numerical dispersion relation and dissipation rate of DSEM for the fourth-order scheme (PN = 4). On the *left*, the *red thick line* shows the exact dispersion relation in a homogenized material $\tilde{\omega} = \pm\tilde{k}$ along with the real value of the non-dimensional frequency plotted against the non-dimensional wave number ($\tilde{k}$). On the *right*, the imaginary value of the non-dimensional frequency (Im $\{\tilde{\omega}\}$) is plotted with respect to the non-dimensional wave number ($\tilde{k}$). (Color figure online)

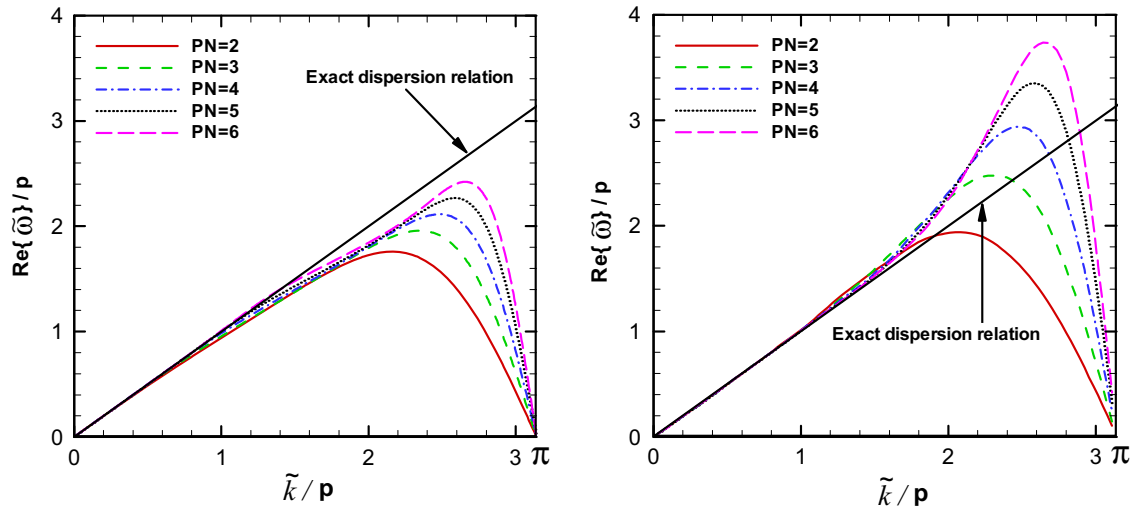

Fig. 5 Numerical dispersion relation of the only physical mode normalized by the polynomial order (p) for two schemes (DSEM (*left*) and DGM (*right*)) in the homogeneous material

persion provided by the theoretical solution. The numerical solution is a superposition of $N \times (p + 1)$ waves traveling at different phase velocities: two are the physical modes with the frequency that approximates the exact dispersion relation for a range of wavenumbers, $\tilde{\omega} = \pm\tilde{k}$ where $\tilde{k} = k\delta$ and $\tilde{\omega} = \omega\delta/c$ are the non-dimensional wave number and frequency, respectively, and the phase speed is unity in this case and the positive and the negative signs mean the right- and the left-going waves, respectively. The others are the parasite modes associated with the numerical scheme.

Figure 4 represents numerical dispersion relations and numerical dissipation rates in the semi-discretization of the one-dimensional elastic wave equations for the fourth-order DSEM scheme. In this figure, two physical modes and eight parasite modes are observed in DSEM. The physical modes agree well with the exact dispersion relation up to approximately $\tilde{k} = 3$ in DSEM. At higher frequency, the curve of a physical mode in DSEM is below the exact dispersion relation line ($\tilde{\omega} = \tilde{k}$). This means that higher wave components produced numerically during the simulation lag behind the physical wave in DSEM. In DSEM, the dissipation rate of the parasite modes is relatively large for the resolved range of wave numbers. Therefore, it will quickly damp out as the wave propagates in space creating a numerically stable solution.

Figure 5 shows the numerical dispersion relation of the only physical mode of a right-going wave for both DSEM and discontinuous Galerkin method (DGM) schemes of order 2–6

Table 1 Maximum resolvable wave number and its relation to wave frequency

Order (NP)	$k_c\delta$	PPW	$\omega_c l$	$k_c l$
1	0.18	70	3.14	0.36
2	0.72	26	3.14	1.44
3	1.56	16.1	3.14	3.12
4	2.44	12.9	3.14	4.88
5	3.58	10.5	3.14	7.16
6	4.86	9.0	9.42	9.72
7	6.06	8.3	15.71	13.56
8	7.66	7.4	15.71	15.32

for comparison. The details of DGM scheme are given in the reference [24]. For the purpose of comparison between the schemes of different orders, the wavenumber $\tilde{k}$ is normalized by the PN of the scheme P. It is apparent from this figure that a wave in a DSEM solution lags behind the true wave, and the overshoot in the DGM solution implies the waves for larger wave numbers lead the true wave.

To quantify the resolution of the scheme, the following criterion is often used [24,26,27]

$$\left|\tilde{\omega}_{real} - \tilde{k}\right| < 0.01 \quad \text{and} \quad \left|\tilde{\omega}_{imag}\right| < 0.01. \tag{38}$$

This criterion ensures that the dispersion and the dissipation errors are less than 1.0 %. Table 1 represents the resolution property of the scheme. Here, k_c is the maximum resolvable wavenumber and the corresponding number of points per wavelength (PPW) is defined by $2\pi(p+1)/k_c\delta$, which is the minimum number of points to represent the smallest wavelength of the waves satisfying Eq. (38). For example, this scheme incurs an error of less than 1.0 % when 9 mesh points per wavelength for the sixth-order scheme is used in the computation.

The dispersion and the dissipation errors in the semi-discretization of the one-dimensional elastic wave equations in a homogeneous material can be also observed in the application of the Floquet–Bloch theory discussed in Sect. 3.1. Figure 6 represents the elastic band structure for longitudinal elastic wave modes propagating in a one-dimensional infinite homogeneous system. According to the Bloch theory with an artificial periodicity l, all the curves can be represented in the one-dimensional Brillouin zone. As the Brillouin zone ($\mu = \pm\pi/l$) is symmetrical about the y-axis, we plot only half of the Brillouin zone ($0 \le \mu \le \pi/l$) [5,6]. In this case, the structure is assumed homogeneous and it does not lead to the stop band structure. It means that all the waves applied to the material propagate without attenuation (pass band). Also it is observed that the slope in this figure is unity which is the same as the phase velocity of the elastic wave, as expected. Compared to Fig. 4, all the curves in Fig. 6 represent a linear relation due to the physics of wave propagation in the Floquet–Bloch theory. The discrepancy between the analytic solution and the numerical result is observed at the boundaries ($\mu = \pm\pi/l$ and $\mu = 0$) and it is dependent upon the numerical accuracy, i.e., the PN in the DSEM. As the order increases, Fig. 7 shows that these errors exponentially decrease with an exponential decay constant of unity. An analytic dispersion relation (Eq. (23)) yields an infinite number of frequencies $\tilde{\omega}$, while the numerical dispersion relation, Eq. (37), naturally yields a finite number of frequencies, which depends on the PN of the DSEM as shown in Figs. 6, 9, and 13. The large discrepancy between the numerical and the analytic results particularly for large frequencies motivated this study. Even though one can find numerical solutions from Eq. (37) in real complicated geometries in 2D or 3D, they will entail large errors, particularly for larger frequencies, which cannot be ascertained *a priori*. Then determining the largest frequency where a numerical method under consideration resolves with specified accuracy is of practical importance. This maximum resolvable frequency $\tilde{\omega}_c$ for a given order of the DSEM is presented in Tables 2, 3 and 4.

To quantify the resolution of the DSEM scheme, the following criterion is used

$$|\omega^{(n)} l - \omega^{(a)} l| < 0.01, \tag{39}$$

where $\omega^{(n)}$ and $\omega^{(a)}$ are the numerical and analytic angular frequencies for a given μ in the range 0 to $\mu = \pi/l$, respectively. If the criterion of Eq. (39) is satisfied, then the numerical errors will be less than 1.0 %. Table 1 represents the resolution property of the scheme. Here, ω_c is the maximum resolvable angular frequency satisfying Eq. (39). In Table 1, ω_c's are shown to be discrete values defined at the right boundary ($\mu = \pi/l$). Also, numerical errors in each line are constant and are accumulated in the next neighboring folded line, which are shown in Fig. 6. In Table 1, the last column represents $k_c l$ determined from $k_c\delta$ where $\delta = l_1$ and $l_1/l = 0.5$. In this case, the wave velocity is $c^{(1)} = c^{(2)} = 1$ and so $\omega_c = k_c$. It is difficult to generalize the relation between $\omega_c l$ and $k_c l$ but there is a tendency that for higher order DSEM of PN greater than or equal to 6, the numerical result of $\omega_c l$ tends to $k_c l$. This means that the errors in $\omega_c l$ come from the numerical dispersion and dissipation errors of DSEM. It implies that the maximum resolvable frequency (ω_c) in the Floquet–Bloch analysis is determined by the maximum resolvable numerical wavenumber (k_c). Figure 7 represents numerical dispersion errors for the solution of the elastic homogeneous material with different PNs. The numerical value of ωl is chosen at the first right boundary to compute the error defined by $|\omega^{(n)} l - \omega^{(a)} l|$. This figure shows an exponential decay of the error.

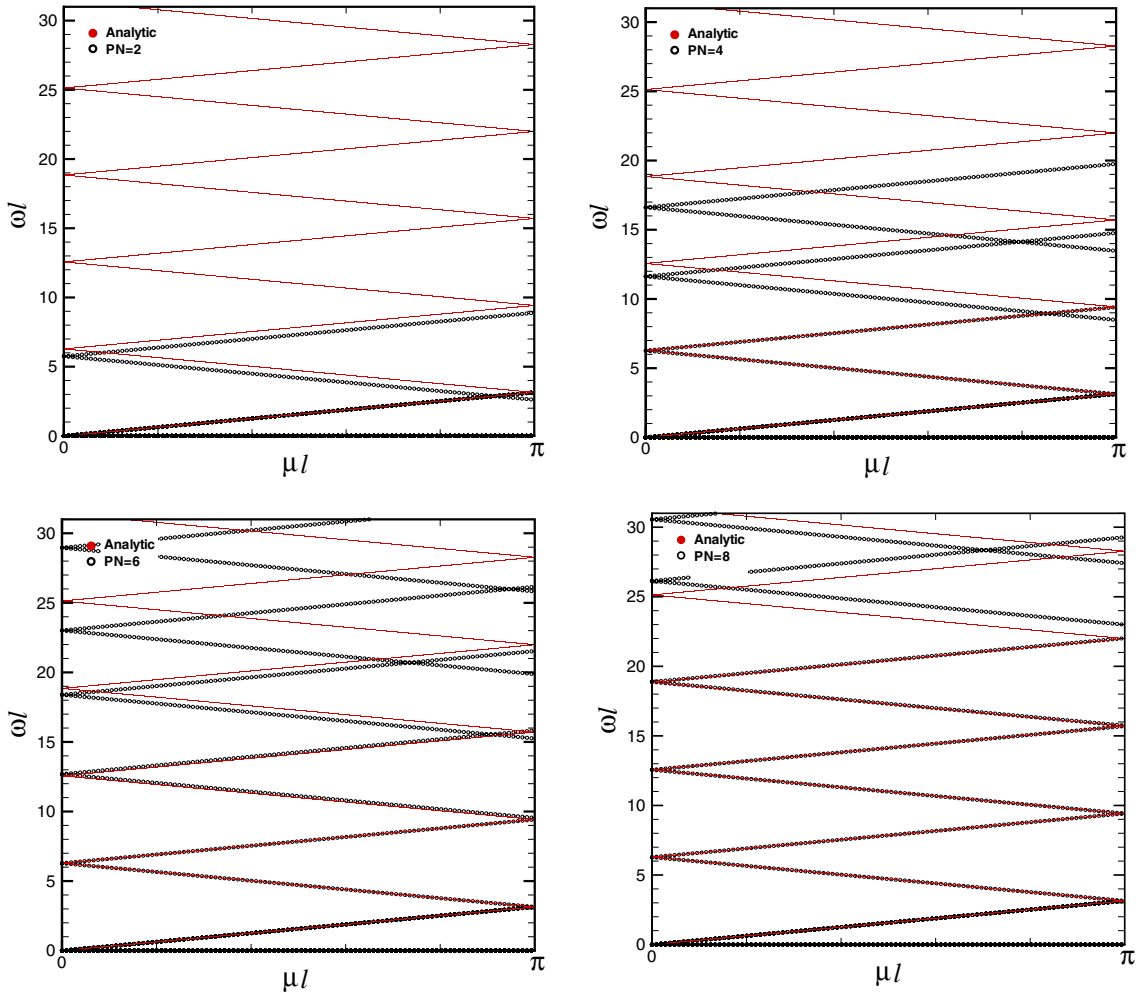

Fig. 6 Elastic band structure for longitudinal elastic wave modes propagating in a onedimensional infinite homogeneous system. The analytic solution is compared to polynomial orders (PN) 2, 4, 6, and 8

4.2 Wave propagation in a periodic heterogeneous material

4.2.1 Case 1: $Z_1 \neq Z_2$ and $c^{(1)} = c^{(2)}$

In this section, we analyze the dissipation and the dispersion errors in a periodic heterogeneous material characterized by the parameters $\rho^{(1)} = 1$, $K^{(1)} = 1$, $\rho^{(2)} = 3$, and $K^{(2)} = 3$ which result in $Z_1 = 1$, $Z_2 = 3$, and $c^{(1)} = c^{(2)} = 1$. For convenience, the volume ratio from Fig. 2 is $\beta = l_1/l = 0.5$. Figure 8 represents the elastic band structure for longitudinal elastic wave modes propagating in a one-dimensional infinite periodic heterogeneous system with layers of two elastic materials. Compared to the homogeneous case, the stop bands are clearly seen on the right boundary of this figure as already illustrated in Fig. 3. All the frequencies lying on the stop bands, such as $\omega l = 3$, 10, 15, would attenuate as they propagate through the periodic material. The accuracy of the band structure naturally depends upon the polynomial order (PN) as shown in Fig. 8. Figure 9 illustrates the elastic band structure for eight different PNs. This figure highlights the accuracy between the analytic and the numerical results through comparisons with the Floquet–Bloch theory. Increased numerical accuracy is shown to strongly depend upon the PN in the DSEM.

Table 2 represents the maximum resolvable angular frequency satisfying Eq. (39) for several different PNs in the DSEM. Due to the existence of the stop band, it is challenging to determine the exact maximum resolvable angular frequency in case of PN = 4, 5 or PN = 8, 9 since it may be located on the stop band. The last column in Table 2 represents the stop bands in the present periodic material. According to this result, $\omega_c l$'s in both PN = 4, 5 and PN = 8, 9 are 2.10 and 14.65, respectively, which are the frequencies at the right boundary ($\mu l = \pi$) in Fig. 8. Results from Table 2 are plotted in Fig. 10 to illustrate that there is a jump in the maximum resolvable frequency near the PN of 6. The results illustrate a step-like increase with respect to PN within this range of PN order. On the interval between PN = 5 and 7 there is a large

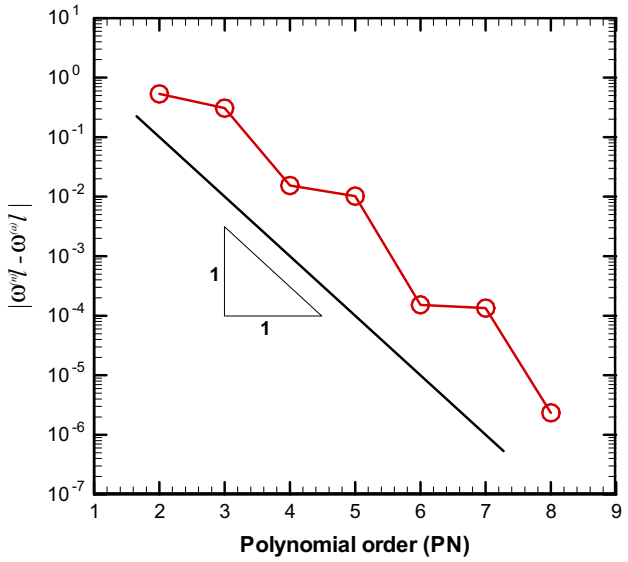

Fig. 7 Numerical errors for different polynomial orders in DSEM. The absolute error was obtained at the first right boundary $\mu = \pi/l$

Table 2 Maximum resolvable frequency with respect to the polynomial order and stop band obtained from the present periodic material ($Z_1 = 1,\ Z_2 = 3$ and $c^{(1)} = c^{(2)} = 1$)

Order (NP)	$\omega_c l$	Stop band
2	0.90	2.10–4.19
3	1.71	8.38–10.47
4	2.10	14.65–16.75
5	2.10	⋮
6	8.23	
7	14.03	
8	14.65	

Table 3 Maximum resolvable frequency with respect to the polynomial order and stop band obtained from the present periodic material ($Z_1 = 1,\ Z_2 = 0.5$ and $c^{1} = c^{(2)} = 1$)

Order (NP)	$\omega_c l$	Stop band
2	1.30	2.46–3.82
3	2.04	8.75–10.11
4	3.82	15.03–16.39
5	3.82	⋮
6	8.58	
7	10.11	
8	16.39	

increase in the slope between $\omega_c l$ and the PN which provides insight in numerical computation accuracy and efficiency. For example, if one is only interested in the response in the low frequency regime, the choice of PN = 3 or 4 will be sufficient but for higher frequency PN = 7 or 8 is ideal.

Table 4 Maximum resolvable frequency with respect to the polynomial order (PN) in case 2

Order (NP)	$\omega_c l$	Order (NP)	$\omega_c l$
2	1.26^{R}	9	5.03^{L}
3	1.26^{R}	10	6.28^{R}
4	1.26^{R}	11	6.28^{R}
5	3.63	12	8.54
6	3.28	13	8.80^{R}
7	3.77^{R}	14	8.80^{R}
8	4.43	15	10.03

L/R left and right boundaries, respectively

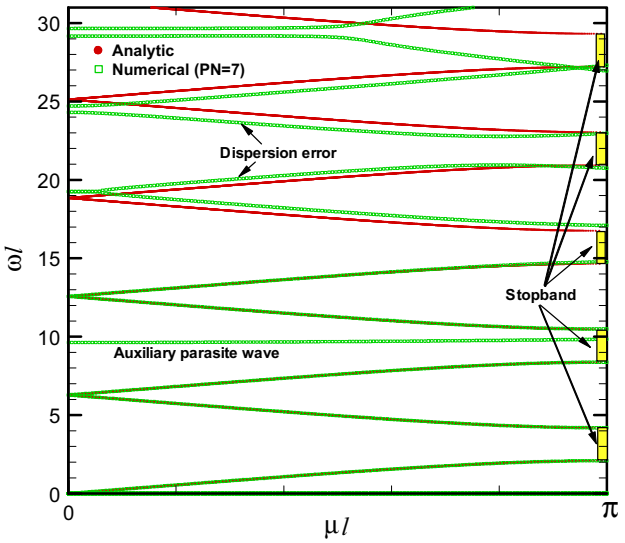

Fig. 8 Comparison of elastic band structure for longitudinal elastic wave modes propagating in a one-dimensional infinite periodic heterogeneous system with layers of two elastic materials between the analytic solution and the numerical result for PN = 7 (Case 1: $Z_1 = 1,\ Z_2 = 3$ and $c^{(1)} = c^{(2)} = 1$)

Figure 11 represents maximum resolvable frequency versus the order of the polynomial (PN) based on the criterion given by Eq. (39) for $\rho^{(1)} = 1,\ K^{(1)} = 1,\ \rho^{(2)} = 0.5$, and $K^{(2)} = 0.5$. These parameters give $Z_1 = 1,\ Z_2 = 0.5$, and $c^{(1)} = c^{(2)} = 1$. Similar to Fig. 10, the stop bands in Figure 11 exist on the right boundary but narrower than those in Fig. 10. The stop bands are also given in Table 3. Compared to Fig. 10, on the interval between PN = 5 and 7 $\omega_c l$ shows an increase in the slope between $\omega_c l$ and the PN. In regions between PN = 5 and 6 or PN = 7 and 8, $\omega_c l$ rapidly increases. However, $\omega_c l$ is the same at PN = 4 and 5 or PN = 8 and 9 and therefore provide guidance to trade-offs in accuracy and computational efficiency.

Figure 12 plots the numerical error for the two heterogeneous elastic band gap solutions using DSEM with dif-

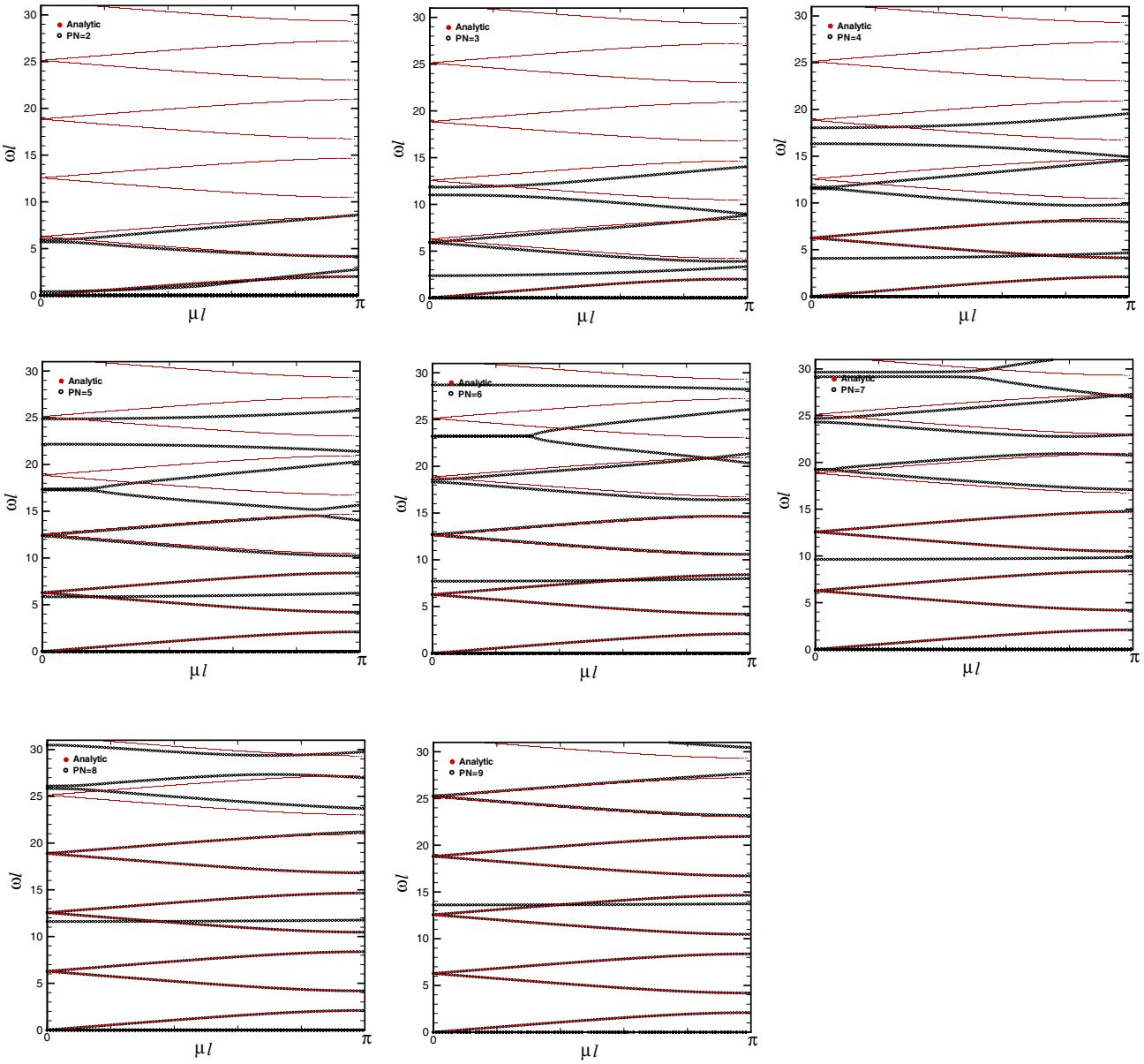

Fig. 9 Elastic band structure for longitudinal elastic wave modes propagating in a onedimensional infinite periodic heterogeneous system with layers of two elastic materials (Case 1: $Z_1 = 1$, $Z_2 = 3$ and $c^{(1)} = c^{(2)} = 1$). Numerical errors due to polynomial (PN) order 2 to 9 are shown

ferent PNs. The numerical value of ωl at the first right boundary was chosen to compute the absolute error in Fig. 12a. These errors show a nominal exponential decay with respect to PN but an odd number of PN does not reduce the error as much as an even number of PN. We integrate the error for all the points on the dispersion curve that are resolvable with the lowest polynomial order simulated (PN=2). When the squared error is summed up to the maximum $\omega^{(n)} l$ computed for PN=2, we find that the error follows a much smoother curve (see Fig. 12b). The exponential decay rate of the error was also seen in the homogeneous case (Fig. 7). This means that the numerical solution in this problem reflects the characteristics of the exponential decay with respect to PN obtained by the DSEM.

4.2.2 Case 2: $Z_1 = Z_2$ and $c^{(1)} \neq c^{(2)}$

The last case we consider contains a uniform impedance but the wave speed in each domain, $\Omega_n^{(1)}$ and $\Omega_n^{(2)}$, varies. Parameters used here include $\rho^{(1)} = 4$, $K^{(1)} = 0.25$, $\rho^{(2)} = 1$, and $K^{(2)} = 1$ which results in $c^{(1)} = 0.25$, $c^{(2)} = 1$ and $Z_1 = Z_2 = 1$. The volume ratio is again fixed to $\beta = l_1/l = 0.5$. This example does not lead to the band gap structure since the impedance is the same in a whole domain. Therefore, it is much closer to the homogeneous case in

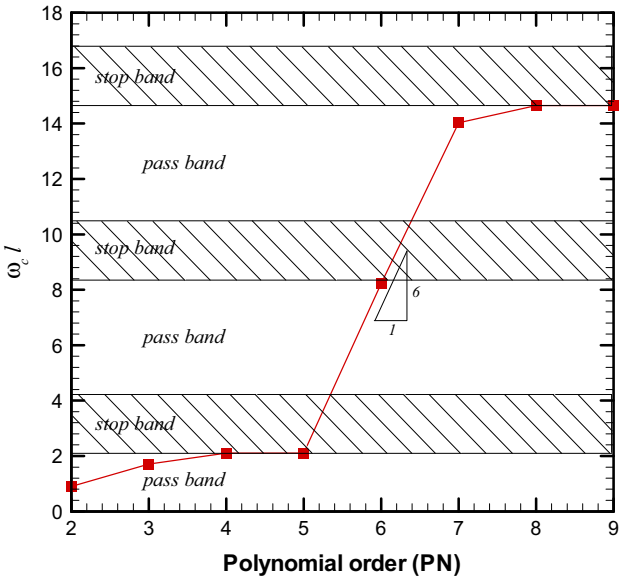

Fig. 10 Maximum resolvable frequency with respect to the polynomial order (PN) in DSEM in Case 1 ($Z_1 = 1$, $Z_2 = 3$ and $c^{(1)} = c^{(2)} = 1$)

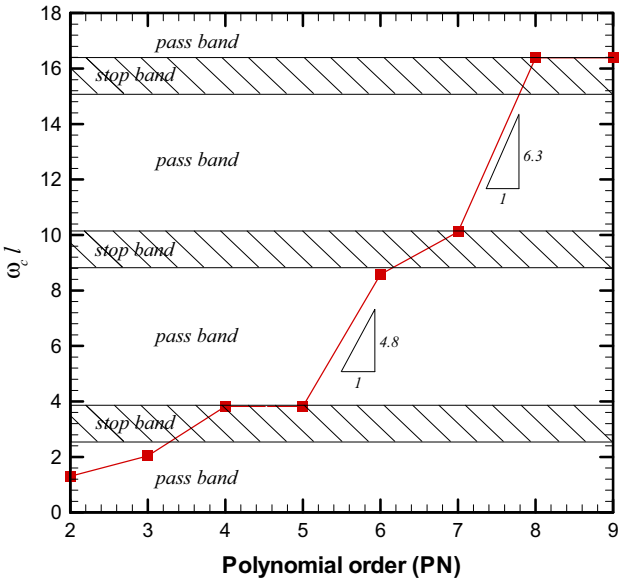

Fig. 11 Maximum resolvable frequency with respect to the polynomial order (PN) in DSEM in Case 1 ($Z_1 = 1$, Z_2 0.5 = and $c^{(1)} = c^{(2)} = 1$)

Sect. 4.1. But, the elastic wave propagates with different velocities in each periodic domain. Figure 13 represents the elastic band structure for Case 2. Similarly to the homogenized case, there are folded and continued zig-zag linear lines between 0 and π in the x-axis and their slopes describe the effective sound speed of the periodic medium, Θ_1, which can be derived from homogenization theory. According to [40,41], the homogenized relation is

$$\Theta_1^2 = \frac{\bar{K}}{\bar{\rho}} = \frac{[\beta/K^{(1)} + (1-\beta)/K^{(2)}]^{-1}}{[\beta\rho^{(1)} + (1-\beta)\rho^{(2)}]}, \tag{40}$$

where $\bar{\rho}$ and $\bar{K}$ are the effective density computed by arithmetic averaging and Young's modulus obtained by harmonic averaging of densities and Young's moduli in Ω_n, respectively. The effective sound speed Θ_1 computed from Eq. (40) is 0.4. In Fig. 13, the numerical results with different PNs are compared with the analytical solution. It is shown that as the PN increases, the accuracy is also increased. Table 4 represents the maximum resolvable frequency with respect to the PN for this case of variable wave speed. The maximum resolvable frequency is determined by the criterion of Eq. (39). Figure 14 represents the relation between the maximum

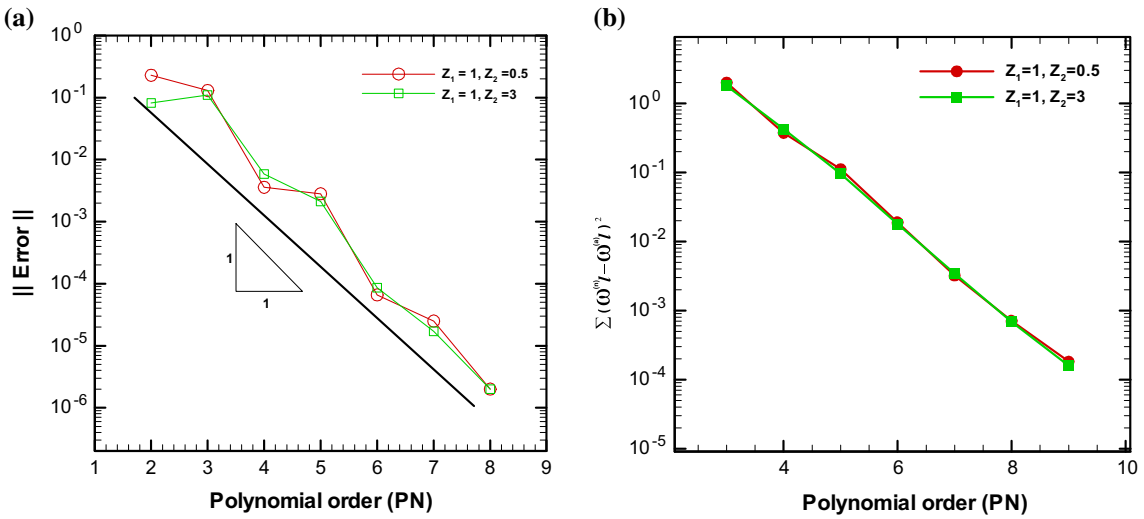

Fig. 12 Numerical error for the solution of elastic band gap problem with different polynomial orders: **a** the absolute error was computed at the *first right* boundary, **b** the *squared error* was summated up to the maximum $\omega^{(n)}l$ computed for PN = 2

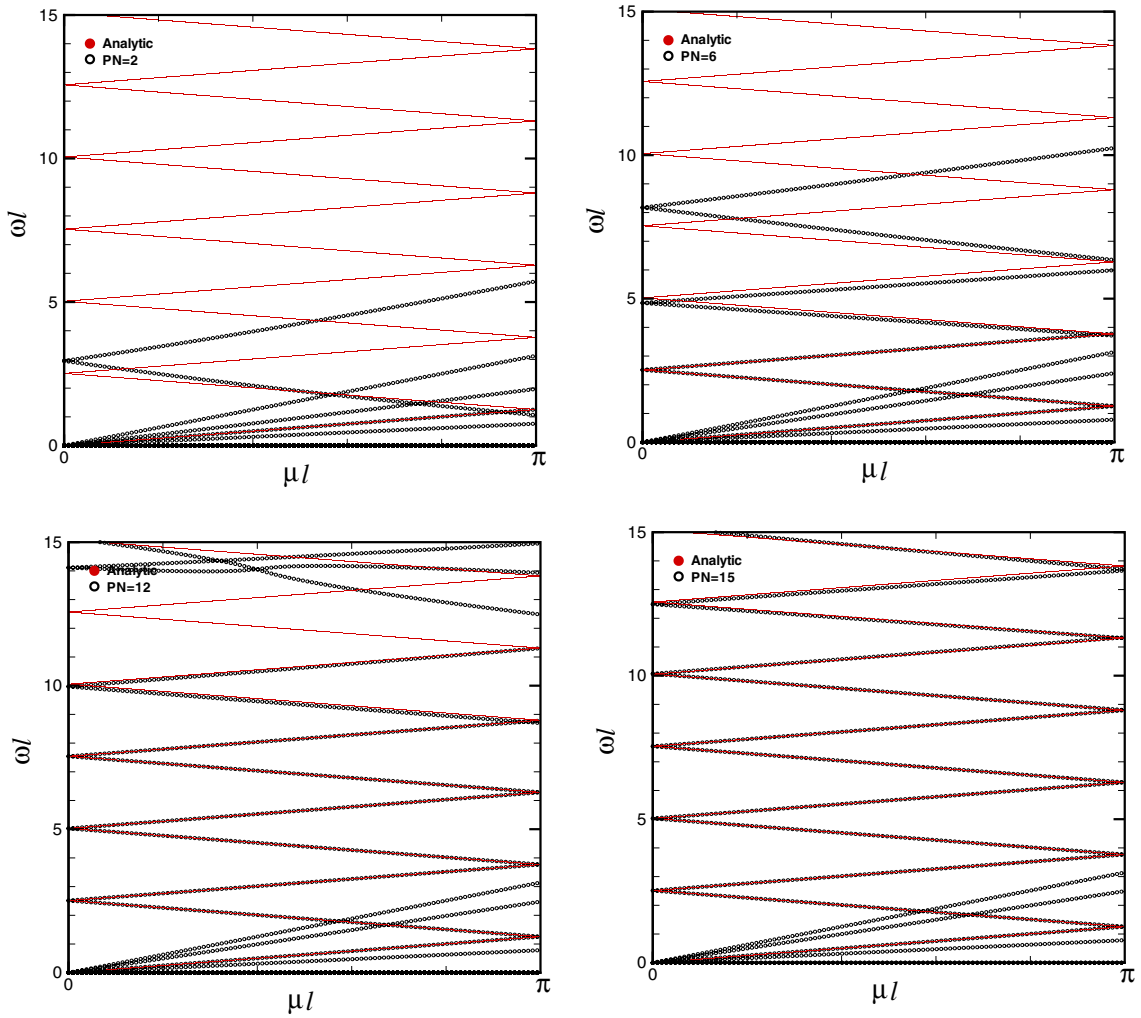

Fig. 13 Elastic band structure for longitudinal elastic wave modes propagating in a onedimensional infinite periodic heterogeneous system with layers of two elastic materials (Case 2)

resolvable frequency and the PN. In Fig. 14, the left and the right boundaries denote the position at $\mu l = 0$ and $\mu l = \pi$, respectively. Similar to the previous two cases of heterogeneous materials, there is a significant increase in $\omega_c l$ at PN = 5 and 12 for materials with discontinuous wave speeds in each regime. While it is not trivial to generalize the behavior in Fig. 14, it is important to point out that the significant jump in $\omega_c l$ happens at the right boundaries ($\mu l = \pi$).

Figure 15 represents zoomed elastic band structure for low longitudinal elastic wave modes in Case 2. In this figure it is observed that there are four different slopes originated from the origin and they all disappear at the right boundary. The frequency (ω) where this phenomenon happens is low compared to the effective wavenumber (μ) since $\omega < \mu$. In this figure, all the curves numbering ① through ④ are linear and their slopes represent the wave propagation velocities. Number ① denotes the effective sound speed Θ_1 with the value of 0.4. Numbers ② and ③ represent $c^{(1)} = 0.25$ and $c^{(2)} = 1$, respectively. These physical waves (①∼③) agree well with the exact dispersion relation up to $\mu l = \pi$ for three different PNs. Number ④ represents parasite mode dependent upon PN in the DSEM since the imaginary values of ω on this line are negative and approximately -10. The dissipation rate of this parasite mode is relatively large for the resolved range of wave numbers. Therefore, it will quickly dampen out as the wave propagates in space.

5 Concluding remarks

The numerical dispersion and dissipation properties of the DSEM have been quantified for elastodynamic problems containing one dimensional periodic heterogeneous microstructure. To calculate and compare complex dispersion relations in heterogeneous materials, the Floquet–Bloch theory was used. Their frequency dependent characteristics and their elastic band behavior were numerically studied by comparison with the analytic solution.

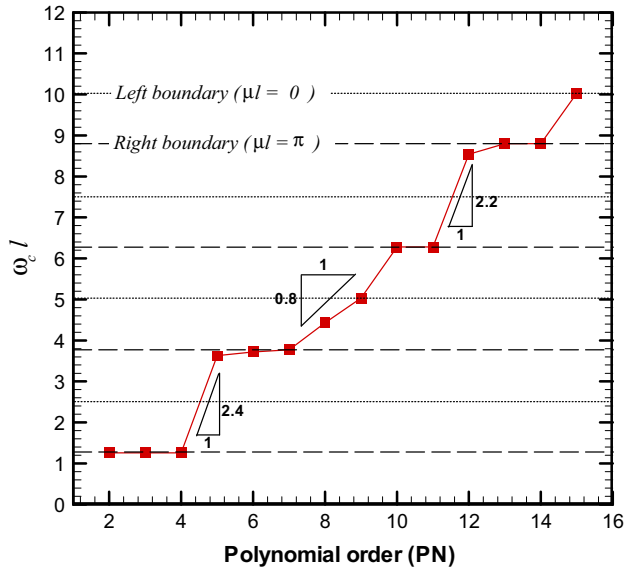

Fig. 14 Relation between the maximum resolvable frequency and the polynomial order for Case 2

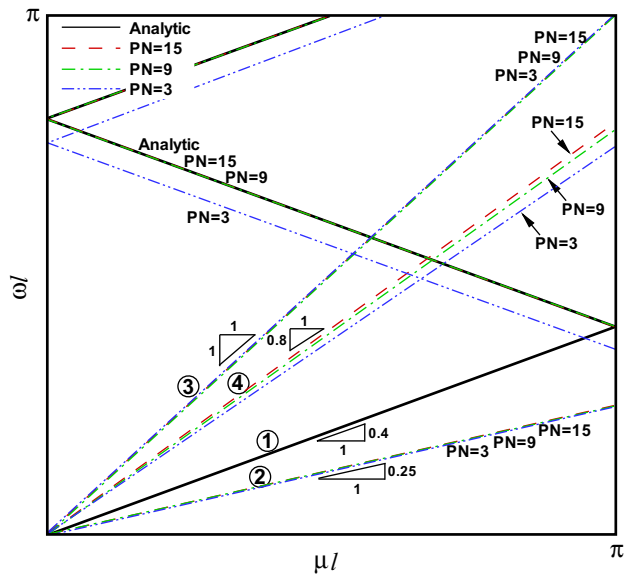

Fig. 15 Zoomed elastic band structure for low longitudinal elastic wave modes in Case 2

The accuracy of the dispersion relation was investigated with respect to the spectral polynomial orders for three different materials: a homogeneous material as a benchmark and two different types of heterogeneous materials. For the homogeneous material, the theoretical solution of constant wave speed with respect to frequency was compared with the numerical solutions given errors that nominally decayed exponentially. A larger jump in errors occurred at the right Brillouin zone boundaries. For the second case with different impedances in each domain, it was found that there is a discontinuous jump of the maximum resolvable frequency within the pass bands resulting in a step-like increase of the maximum resolvable frequency with respect to PN. This investigation provides insight in the existence of the optimal PNs for accurate computations of the elastic band structures.

Lastly, for the last case in which the wave speed in each domain differs, there are folded and continued zig-zag linear lines in the first Brillouin zone. In the low frequency regime, there exist four different wave speed components: two physical wave speeds in each domain, the effective sound speed, and the parasite wave speed which is dependent upon the polynomial order in DSEM. But, in the higher frequency region, there only exists the effective sound speed that is governed by the homogenized material characteristics.

Acknowledgments The authors gratefully acknowledge support through the Federal Aviation Administration Center of Excellence on Commercial Space Transportation through FAA Grant 029994.

Appendix

We derive the numerical dispersion relation of DSEM scheme chosen to simulate the elastic wave propagation through homogeneous materials in this study. Equation (12) can be expressed in the matrix form

$$\frac{\delta}{2}\mathbf{Q}\frac{\partial \mathbf{C}^n}{\partial t} + \mathbf{N}_{-1}\mathbf{C}^{n-1} + \mathbf{N}_0\mathbf{C}^n + \mathbf{N}_1\mathbf{C}^{n+1} = 0, \tag{41}$$

where $\mathbf{C}^n = [\mathbf{C}_0^n, \mathbf{C}_1^n, \ldots, \mathbf{C}_\mathrm{p}^n]^\mathrm{T}$. Here, $\mathbf{A}_\mathrm{L}^{n-1} = \mathbf{A}_\mathrm{L}^n$ and $\mathbf{A}_\mathrm{R}^{n+1} = \mathbf{A}_\mathrm{R}^n$ since the medium is homogeneous. If the element is uniform in one dimension, then we can seek solutions of the form

$$\mathbf{C}^n = \tilde{\mathbf{C}}\mathrm{e}^{\mathrm{j}(\omega t - kn\delta)}, \tag{42}$$

where $\tilde{\mathbf{C}}$ is a complex vector of dimension $[\mathrm{N}\times(\mathrm{p}+1)]$. The substitution of Eq. (42) into (41) gives an algebraic system for $\tilde{\mathbf{C}}$

$$\left(\frac{\mathrm{j}\omega\delta}{2}\mathbf{Q} + \mathrm{e}^{\mathrm{j}k\delta}\mathbf{N}_{-1} + \mathbf{N}_0 + \mathrm{e}^{-\mathrm{j}k\delta}\mathbf{N}_1\right)\tilde{\mathbf{C}} = 0. \tag{43}$$

If we define the non-dimensional wave number and frequency as $\tilde{k} = k\delta$ and $\tilde{\omega} = \omega\delta/c$ where $c = \sqrt{K/\rho}$, Eq. (43) has a non-trivial solution when the determinant of the following matrix is zero, which leads to the numerical dispersion relation given by

$$\det\left(\frac{\mathrm{j}c\tilde{\omega}}{2}\mathbf{Q} + \mathrm{e}^{\mathrm{j}\tilde{k}}\mathbf{N}_{-1} + \mathbf{N}_0 + \mathrm{e}^{-\mathrm{j}\tilde{k}}\mathbf{N}_1\right) = 0, \tag{44}$$

where

$$\{Q\}_{lm} = \mathbf{I}\int_{-1}^{1} L_l(\xi)L_m(\xi)\mathrm{d}\xi,$$

$$\{N_0\}_{lm} = \mathbf{A}^n_{\mathrm{L}} L_l(1) L_m(1) - \mathbf{A}^n_{\mathrm{R}} L_l(-1) L_m(-1) - \mathbf{A}^n \int_{-1}^{1} L_m(\xi) \frac{\partial L_l(\xi)}{\partial \xi} \mathrm{d}\xi,$$
$$\{N_{-1}\}_{lm} = -\mathbf{A}^n_{\mathrm{L}} L_m(1) L_l(-1),$$
$$\{N_1\}_{lm} = \mathbf{A}^n_{\mathrm{R}} L_m(-1) L_l(1),$$
$$\text{where } l, m = 0, 1, \ldots, \mathrm{p}. \tag{45}$$

References

1. Joannopoulos JD, Meade RD, Winn JN (1995) Photonic crystals: molding the flow of light. Princeton University Press, Princeton
2. Kushwaha MS (1996) Classical band structure of periodic elastic composites. Int J Mod Phys B 10:977–1094
3. Kushwaha MS (1999) Band gap engineering in phononic crystals. Recent Res Dev Appl Phys 2:743–855
4. Sigalas M, Kushwaha MS, Economou EN, Kafesaki M, Psarobas IE, Steurer W (2005) Classical vibrational modes in phononic lattices: theory and experiments. Z Kristallogr 220:765–809
5. Stroscio MA, Dutta M (2001) Phonons in nanostructures. Cambridge University Press, Cambridge
6. Nelson DF (1979) Electric, optic, and acoustic interactions in dielectrics. Wiley, New York
7. Tamura S, Shields JA, Wolfe JP (1991) Lattice dynamics and elastic phonon scattering in silicon. Phys Rev B 44:3001–3011
8. Liu Z, Chan CT, Sheng P, Goertzen AL, Page JH (2000) Elastic wave scattering by periodic structures of spherical objects: theory and experiment. Phys Rev B 62:2446–2457
9. Penciu RS, Fytas G, Economou EN, Steffen W, Yannopoulos SN (2000) Acoustic excitations in suspensions of soft colloids. Phys Rev Lett 85:4622–4625
10. Russell P, Marin E, Díez A, Guenneau S, Movchan A (2003) Sonic band gaps in PCF performs: enhancing the interaction of sound and light. Opt Express 11:2555–2560
11. Wolfe JP (1998) Imaging phonons: acoustic wave propagation in solids. Cambridge University Press, Cambridge
12. Odeh F, Keller JB (1964) Partial differential equations with periodic coefficients and Bloch waves in crystals. J Math Phys 5:1499–1504
13. Lee EH, Yang WH (1973) On waves in composite materials with periodic structure. SIAM J Appl Math 25:492–499
14. Karim-Panahri K (1983) Antiplane strain harmonic waves in infinite, elastic, periodically triple-layered media. J Acoust Soc Am 74:314–319
15. Angel YC, Achenbach JD (1987) Harmonic waves in an elastic solid containing a doubly periodic array of cracks. Wave Motion 9:337–385
16. Bai D, Keller JB (1987) Sound waves in a periodic medium containing rigid spheres. J Acoust Soc Am 82:1436–1441
17. Sigalas M, Economou EN (1992) Elastic and acoustic wave band structure. J Sound Vib 158:377–382
18. Kafesaki M, Economou EN (1999) Multiple-scattering theory for three-dimensional periodic acoustic composites. Phys Rev B 60:11993–12001
19. Korringa J (1947) On the calculation of the energy of a Bloch wave in a metal. Physica 13:392–400
20. Kohn W, Rostoker N (1954) Solution of the Schrödinger equation in periodic lattices with an application to metallic lithium. Phys Rev 94:1111–1120
21. Taflove A (1998) Advances in computational electrodynamics: the finite-difference time-domain method. Artech House, Norwood
22. Kopriva DA (2009) Implementing spectral methods for partial differential equations: algorithms for scientists and engineers. Springer, Berlin
23. Canuto C, Hussaini MY, Quarteroni A, Zang TA (2006) Spectral methods: fundamentals in single domains. Springer, Berlin
24. Hu FQ, Hussaini MY, Rasetarinera P (1999) An analysis of the discontinuous Galerkin method for wave propagation problems. J Comput Phys 151:921–946
25. Ainsworth M (2004) Discrete dispersion relation for hp-version finite element approximation at high wave number. SIAM J Numer Anal 42(2):553–575
26. Stanescu D, Kopriva DA, Hussaini MY (2000) Dispersion analysis for discontinuous spectral element methods. J Sci Comput 15:149–171
27. Gassner G, Kopriva DA (2011) A comparison of the dispersion and dissipation errors of Gauss and Gauss-Lobatto discontinuous Galerkin spectral element methods. SIAM J Sci Comput 33:2560–2579
28. Åberg M, Gudmundson P (1997) The usage of standard finite element codes for computation of dispersion relations in materials with periodic microstructure. J Acoust Soc Am 102:2007–2013
29. Luo M, Liu QH, Li Z (2009) Spectral element method for band structures of two-dimensional anisotropic photonic crystals. Phys Rev E 79:026705
30. Luo M, Liu QH (2010) Three-dimensional dispersive metallic photonic crystals with a band gap and a high cutoff frequency. J Opt Soc Am A 27(8):1878–1884
31. Ledger PD, Morgan K (2005) The application of the hp-finite element method to electromagnetic problems. Arch Comput Methods Eng 12(3):235–302
32. Jin J (2002) The finite element method in electromagnetics, 2nd edn. Wiley, New York
33. Abeele KV, Broeckhoven T, Lacor C (2007) Dispersion and dissipation properties of the 1D spectral volume method and application to a *p*-multigrid algorithm. J Comput Phys 224:616–636
34. Wiart CC, Hillewaert K (2012) DNS and ILES of transitional flows around a SD7003 using a high order discontinuous Galerkin method. Seventh international conference on computational fluid dynamics (ICCFD7), Big Island, Hawaii
35. Phani AS, Woodhouse J, Fleck NA (2006) Wave propagation in two-dimensional periodic lattices. J Acoust Soc Am 119:1995–2005
36. Cao Y, Hou Z, Liu Y (2004) Finite difference time domain method for band-structure calculations of two-dimensional phononic crystals. Solid State Commun 132:539–543
37. Hussein MI, Hulbert GM, Scott RA (2006) Dispersive elastodynamics of 1D banded materials and structures: analysis. J Sound Vib 289:779–806
38. Toro EF (2009) Riemann solvers and numerical methods for fluid dynamics, 3rd edn. Springer, Berlin
39. Fogarty TR, LeVeque RJ (1999) High-resolution finite-volume methods for acoustic waves in periodic and random media. J Acoust Soc Am 106:17–28
40. Andrianov IV, Bolshakov VI, Danishevs'kyy VV, Weichert D (2008) Higher order asymptotic homogenization and wave propagation in periodic composite materials. Proc R Soc A 464:1181–1201
41. Santosa F, Symes WW (1991) A dispersive effective medium for wave propagation in periodic composites. SIAM J Appl Math 51:984–1005